NRIAG JOURNAL OF ASTRONOMY AND GEOPHYSICS
2022, VOL. 11, NO. 1, 58–68
https://doi.org/10.1080/20909977.2021.2023999

Application of ERT and SSR for geotechnical site characterization: A case study for resort assessment in New El Alamein City, Egypt

Alhussein Adham Basheer and Nouran S. Salama

Department of Geophysics Geology, Faculty of Science, Helwan University, Ain Helwan, Egypt

ABSTRACT

The new city of El Alamein is one of the cities that the Egyptian government seeks to make it a tourist resort area that attract local and international tourism. This study examines how to apply geophysical methods to achieve soil study for foundational and construction purposes, especially near the seacoast. It also seeks to capture evidence of the presence of any clay lenses, as well as the intrusion of seawater into the shallow soil layers. The study uses two effective geophysical methods, the electrical resistivity tomography (ERT) and shallow seismic refraction (SSR). ERT method gained two layers, the appearance of seawater intrusion begins in the second layer. SSR method assigned the same two layers according to the seismic velocities with a thickness close to that determined by the ERT method. From seismic wave velocities, a set of geotechnical properties were calculated. From the integration of all the results, the study area divided into two zones; (1) cohesive soil zone is suitable for construction with low heights, provided that the architectural foundations are placed in the second layer, (2) loose soil and is affected by the intrusion of seawater, so it is not suitable for any construction purposes.

ARTICLE HISTORY
Received 15 September 2021
Revised 25 November 2021
Accepted 25 December 2021

KEYWORDS
Electrical resistivity tomography; shallow seismic refraction; geotechnical properties; seawater intrusion

1. Introduction

The Egyptian state aims to establish new tourist and recreational projects in places characterised by their distance from the old population societies to avoid overcrowding and pollution. Among those projects, a tourist resort project, where the study area lies, is in the new city of El Alamein on the Mediterranean coast. It covers an area of about 20,000 square metres. It lies in latitude between 30°58′29.76” N and 30° 58′34.41”N and in longitude between 28°45′20.59”E and 28°45′26.31” E (Figure 1). The study area, despite its small area, is considered a good case for studying the importance of geophysical measurements that precede the construction process. Geophysical methods are non-destructive and produce quite continuous data over vast areas and, in the saltwater junction zone, in a fast and less expensive way (Goebel et al. 2017; Alabjah et al. 2018). The first method is the electrical resistivity method, which depends on the electrical conductivity of the soil components. The second method is the shallow seismic refraction method, which helps in classifying soil layers based on the change in the density of its components (Comina et al. 2021; Ray et al. 2021).

Both methods reach shallow depths that do not exceed 40 metres. This depth depends on the spatial distances of the sensors (Geophones or electrodes) and other factors represented in the nature of the soil and its components, the sensitivity of the measuring devices, and the power of external sources that generate stimulating energy (ex: hammer, vibration source and generator of electric power) (Basheer et al. 2012; Basheer et al. 2014a; Shynkarenko et al. 2021).

Because the surface of the study area is made of beach sand, it is necessary to know the geotechnical characteristics of the soil layers and the extent of their impact on determining the construction methods and the height of the buildings that are intended and allowed to be built (Sakr et al. 2021). While the proximity of the study area to the sea makes it necessary to be careful to know the effect of the seawater intrusion in the soil, to determine the places of the beginning of this effect and to detect and avoid the presence of any changes in the quality of the soil, such as baby lenses or sabkhas (Alshehri et al. 2021; Satheeskumar et al. 2021). The results of the two measurement methods were divided to obtain the two main purposes of the study, and then an attempt was made to link the results to reach a clear and more comprehensive picture of the nature of the study area.

2. Geological settings

Sedimentary rocks from the Tertiary and Quaternary ages dominated the geologic formations of the main cover of the study area (Shukri et al. 1955; Butzer

CONTACT Alhussein Adham Basheer alhussein.adham@science.helwan.edu.eg Department of Geophysics Geology, Faculty of Science, Helwan University, Ain Helwan, Cairo 11795, Egypt

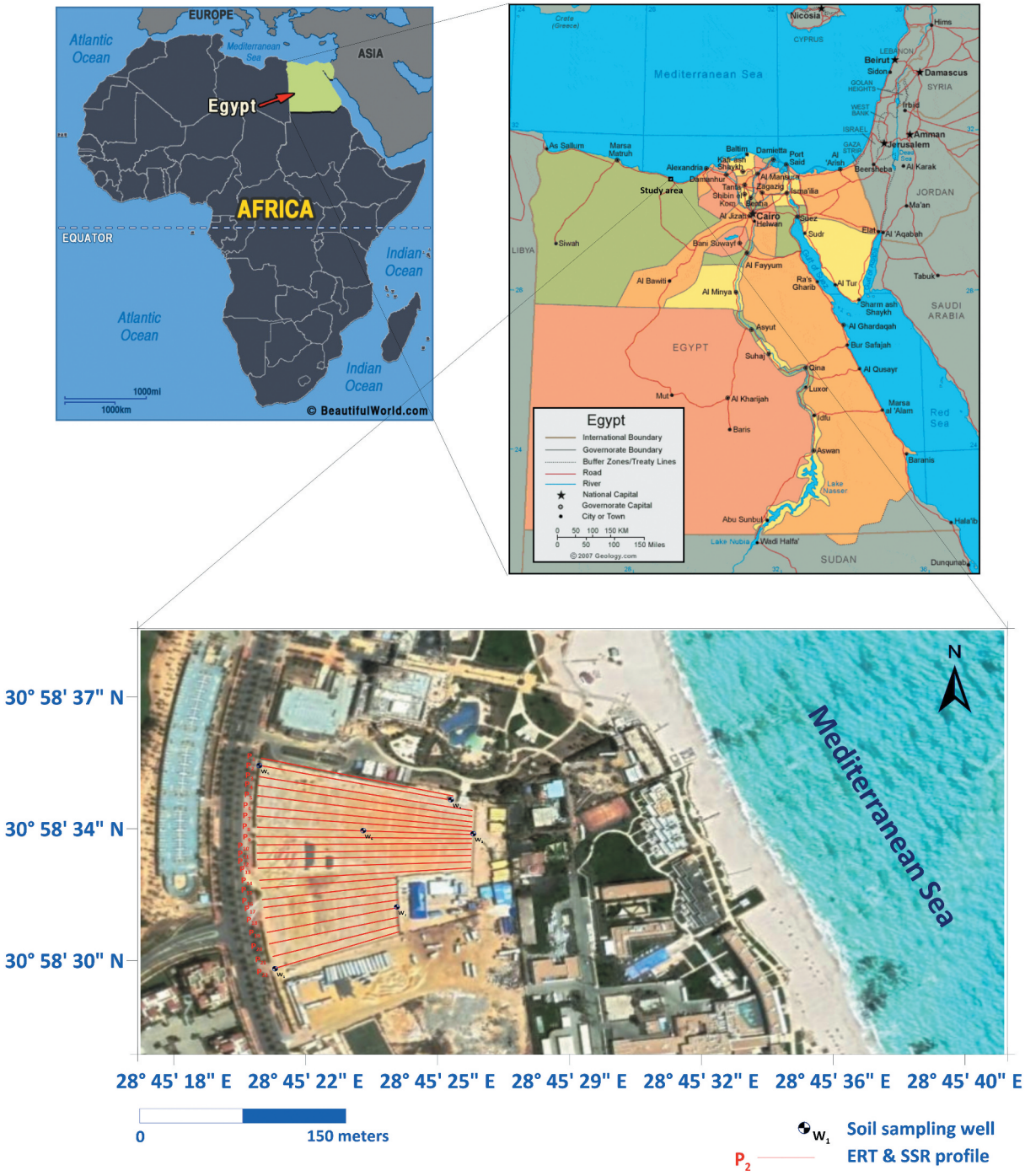

Figure 1. Location map of the study area.

1960; Said 1962, 1990). The coastal plain, wadis, and elevated beaches are almost all exposed to the Quaternary (Figure 2). The Tertiary Pliocene and Miocene are attributed to the large portion of the tableland, whereas the Miocene forms the bed of tableland's surface. The area is composed of a Tertiary Miocene plateau, primarily composed of limestone and sandstone that reaches the shoreline in many spots (Fehlberg and Stahr 1985; El Bastawesy et al. 2008). The Holocene sediments mostly compose coastal sand dunes, lagoon and alluvium, whereas the Pleistocene deposits mainly compose oolitic limestone ridges and ancient lagoon deposits. Except for the coastal ridge, which is typically less cemented, the Quaternary carbonate ridges around the present area are cemented into relatively hard limestone (Zahran 2008).

Tectonically, the northern Western Desert characterises a portion of the tectonic framework of the Egyptian Territory, which is unstable belt (EGPC 1984; Said 1990). The study area and its surrounds have been exposed to numerous tectonic systems ever since the Precambrian time to recent. Precambrian demonstrates three tectonic trends, namely, Nubia (N-S), Red Sea (NNW) and Tibesti (NE) trends. These trends are inbred in the basement rocks of the

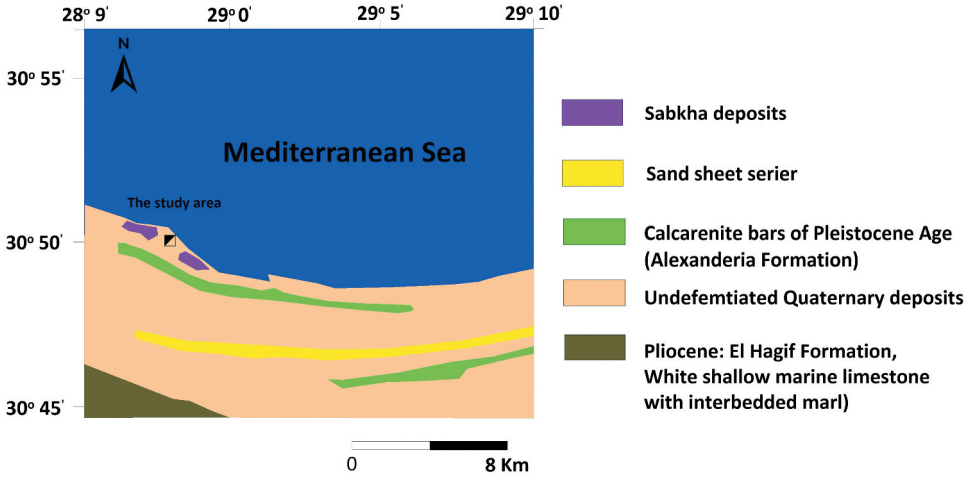

Figure 2. Geological map of the study area and its around.

northern Western Desert (Meshref 1995; BAPETCO 2007). Other E-W tectonic trends appeared in Late Palaeozoic to Late Jurassic (Sultan and Halim 1988). There is another tectonic influence of the Mediterranean region in what is known as the Hellenic Trench (HT). This trench is an oceanic trench that contains the Hellenic subduction zone, directly related to the subduction of the African plate under the Eurasian plate (Gordon et al. 2003; Royden and Papanikolaou 2011; Le Pichon et al. 2019).

3. Methodology

The conventional electrical survey techniques are widely used in groundwater, civil engineering, and environmental investigations since the twenties of the last century. The study area is covered by 22 profiles. Two profiles are 150 metres in length, 12 profiles are 160 metres in length, and 8 profiles are 100 metres in length (Figure 1).

The geoelectrical profiling field data, in the form of electrical resistivity imaging, have been measured by Syscal pro{{year}}. The array configuration of Wenner-Schlumberger has been used in this study, this configuration is characterised by noise reduction and good deeper penetration (Loke et al. 2003) and is widely used in saltwater intrusion investigations (Kazakis et al. 2016). The data have been processed using Res2Dinv software. 3.59, Geotomo Inc{{year}}. using least-square method inversion (Martínez-Moreno 2017). This software is automatically designed to construct two-dimensional resistivity models of the subsurface (Edwards and Hillel 1977; Griffiths and Barker 1993). Concerning the inversion step, the standard Gauss-Newton optimisation method has been used, with a convergent limit of 0.005 (White et al. 2003). All SSR and ERT data have been calibrated by the sampling wells in the study area.

Seismic exploration involves generation of seismic waves and recording the arrival times of these waves from the source to a series of geophones. The motion of the earth surface generated by energy sources is shown in a seismic record. The motion is commonly recorded using instrumental system, including geophone, amplifier, digital recorder and units for monitoring. Conductance of the survey includes different spread systems of geophones. Many techniques can be used to interpret the shallow refraction data. Hawkins (1961) developed the reciprocal, which is the same in nature as Hagiwara's method. Červený et al. (1982) developed the so-called ray method, which has led the ray-tracing technique interpreting seismic data. Recently, Palmer (1980), has invented new method of interpretation, called generalised reciprocal method (GRM) that has many advantages and avoids the complexes of the old methods. The latter technique has been used in computing the data, which is recorded in the present study.

The study area is covered by 22 profiles. Two profiles are 150 metres in length, 12 profiles are 160 metres in length, and 8 profiles are 100 metres in length (Figure 1). Each profile is measured by three different relative positions of the shoot point (Normal, Middle, and reverse arrangement). The shoot point has been placed 0.5 metre near the first geophone. Recording system is called seismograph. The seismograph, which has been used in this study, is "StrataVisor NZXP"{{year}}. The data has been interpreted using several programmes such as (SIP Seisimage Processing{{year}}, Seisviewer{{year}}, and Seisimager/2D{{year}}).

The same places and the same lengths for the 22 profiles were measured in both techniques (Figure 1). This procedure was done for several reasons, such as easily distinguishing between the similarities and differences between the two geophysical techniques, avoiding ambiguity that can exist in the measurements of one of

the two techniques, integrating the two geophysical methods, and reaching for the purpose of exploration and determination of the layers of the study area.

4. Data interpretation and results

4.1. Electric Resistivity Tomography (ERT)

ERT data values are distinct and independent of the place in which they were measured, but the values provide a clear picture of the porosity and permeability of the underlying layers. Laboratory tests of a seawater sample show that it has a very small average resistivity of 0.2 Ohms.m (Nowroozi et al. 1999), while the resistivities of a sand saturated sand sample range between 8 and 50 Ω.m (Adepelumi et al. 2009; Kouzana and Benassi 2010; McInnis et al. 2013; Basheer et al. 2014b).

Generally, the resistivity values have heterogeneity distribution at each horizontal level. The inverted measured data clearly show two layers (Figure 3(a–c)). The first layer is characterised by high values of resistivity with range between about 500 and 815 Ω.m. This layer reflects dry and loose sand with high porosity and permeability in depths from the surface to about 10 to 15 metres depth. The two-dimension maps show the distribution of this layer (Figure 4(a–d)). The resistivity values decrease from north to south in surface and continues to reach depth about 10 metres. These values start to reverse its decreases in depth

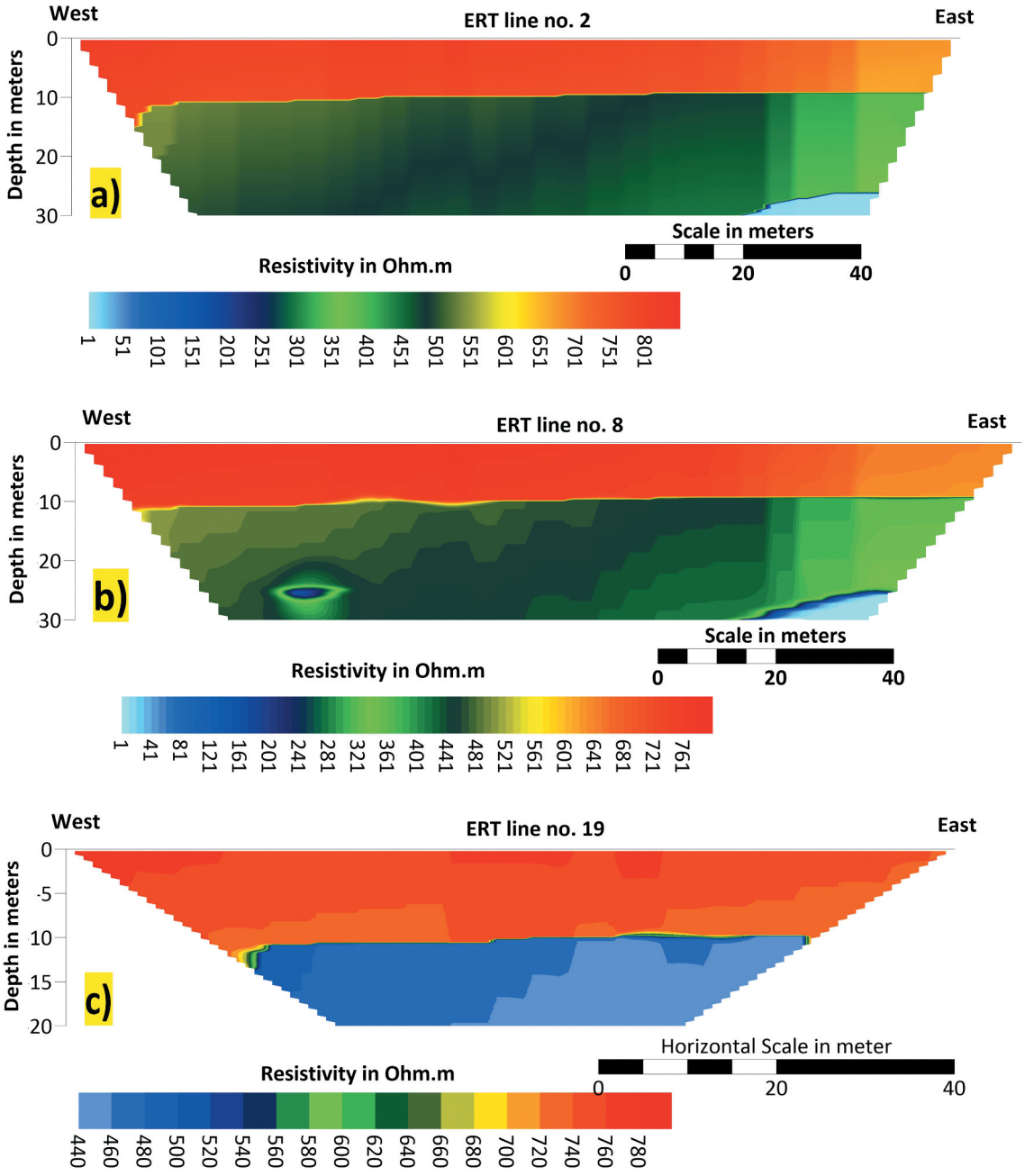

Figure 3. Examples of ERT profile along (a) line 2, (b) line 8, and (c) line 19.

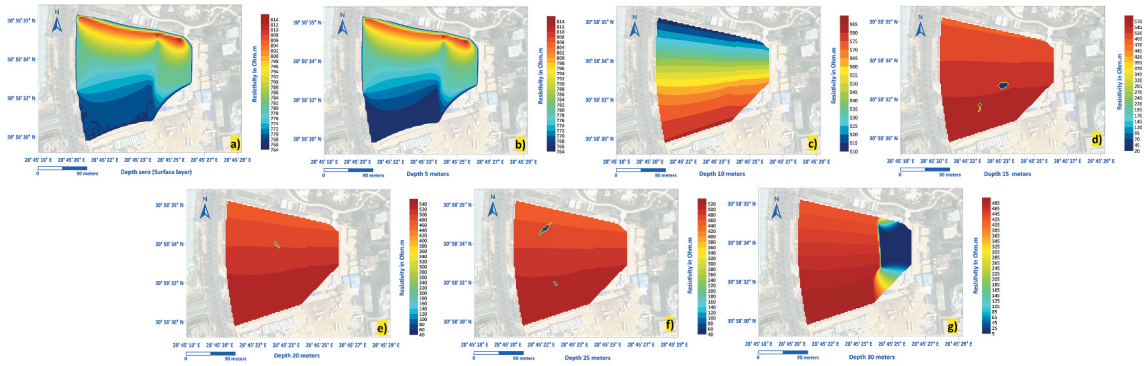

Figure 4. Two-dimensional slices maps at different depths show the distribution of resistivity in (a) surface depth, (b) 5 m depth, (c) 10 m depth, (d)15 m depth, (e) 20 m depth, (f)25 m depth, and (g) 30 m depth.

about 15 metres (Figure d). This behaviour may be due to the interference between two different sand layers. In these depth levels, sands changes to be dry competence sand with low porosity and permeability. There are small and noticeable of gradient change increases towards the east.

The second layer starts to appear in successive deep layers, less than 15 to 30 metres (Figure 3(a–c)). The resistivity values range from 500 to 345 ohms.m. There is a significant decrease in the resistivity value located in the eastern part of the study area (Figure 4(e–g)). These low resistivity values are consistent with the values that result from seawater intrusion into sand. Although the beginnings of this intrusion have been determined from cross-sections (Figure 3(a–c)) and 2-D maps at different depths (Figure 4), it could not be traced at deeper depths of more than 30 metres due to the limitations of data measurement depth related to the length of the horizontal surface array.

The presence of some fragments of some clay sediments that appear in some places at different depths of more than 10 metres should not be overlooked (Figures 3(b) and 4(d–f)). These sedimentary nuggets of clay cannot be described as clay lenses because of their small thickness and extensions. Consequently, this leads to the absence of the need to remove them due to their lack of impact on soil specifications, stability, and suitability for construction operations.

4.2. Shallow seismic refraction

Time-Distance (T-D) curve for Perpendicular (P) and surface (S) waves has been drawn to show the relationship between the first time of seismic signals breaks waves at each geophone and the distance between this geophone and the shoot point, examples of these curves are shown in Figure 5(a,b). The velocity of each segment of T-D curve is defined from the slope of the straight lines, which fits the segment. The interpreted seismic profile illustrates the different layers' parameters as (depths and the different velocities under each geophone). An example of the vertical distribution of P and S waves, as a seismic cross-section of P2, P8, and P19, is shown in Figure 5(c–h). From the interpreted data, it can be distinguished that there are two layers with different speeds in the study area. The first layer consists of cohesionless sand beach, its P waves have velocity ranging between 385 and 453 m/sc. (Figure 6(a)), whereas its S waves have velocity ranging between 130 and 153 m/sc (Figure 6(b)). The thickness of this first layer varies from 10.5 to 14.3 m. The second layer contains sand, and its P waves have velocity varying from 900 to 1130 m/sc. (Figure 6(c)), where its S waves have velocity ranging between 300 and 385 m/sc (Figure 6(d)). The maximum depth of the measurement in most profiles reached about 36 m.

The velocities deduced from the previous interpretations were used to calculate the geotechnical characteristics of the study area.

4.2.1. Geotechnical characteristics

The soil mechanical properties depend on the elastic properties of the rock materials, which may be evaluated from the conventional techniques or from the geophysical measurements (Dutta 1984; Prodehl et al. 1997; Sjogren 2013; Basheer et al. 2014a; Fat-Helbary et al. 2019; Salama et al. 2020). Three general properties were calculated, each property includes the calculation of two mechanical properties of the soil as shown in the following:

4.2.2. Elastic modules

Kinetic Bulk modulus (K) expresses the stress–strain ratio under simple hydrostatic pressure. The following sheriff's equation (1991) has been used to calculate this value:

$$K = E/3(1-2\sigma) = \rho.\left[Vp^2 - -(3/4)Vs^2\right] \quad (1)$$

Its value in the first layer is ranging between 180 in the eastern part and 260 Dyn/Cm^2 in the southwestern part of the study area (Figure 7(a)), whereas in

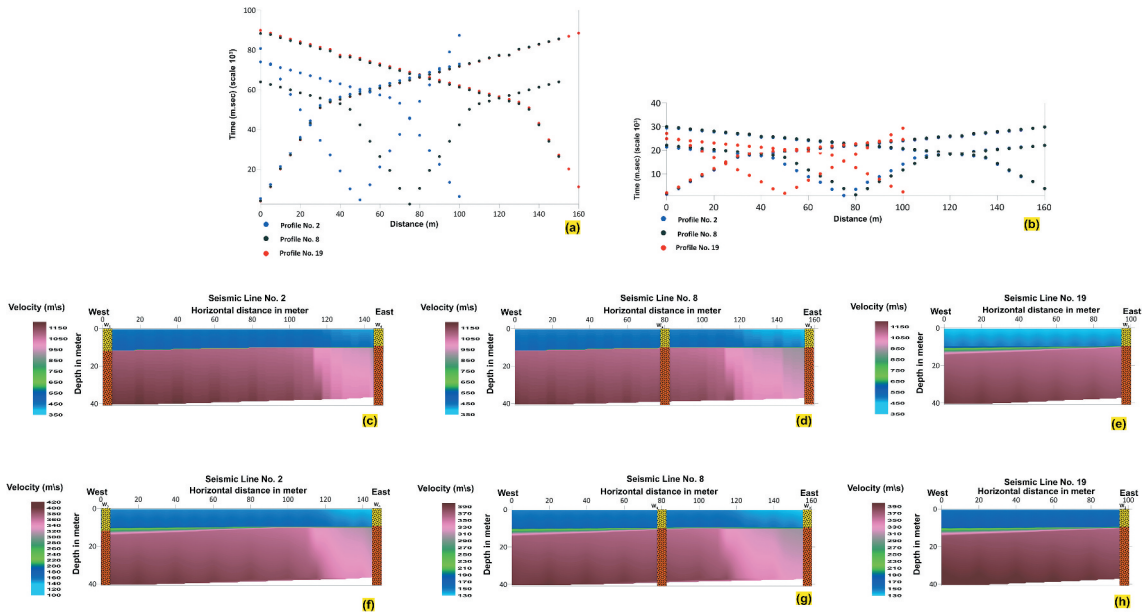

Figure 5. (a) Time–Distance curve of Vp waves, (b) Time-Distance map curve of Vs waves, (c) Vp seismic cross-section of line 2, (d) Vp seismic cross-section of line 8, (e) Vp seismic cross-section of line 19, (f) Vs seismic cross-section of line 2, (g) Vs seismic cross-section of line 8, and (h) Vs seismic cross-section of line 19.

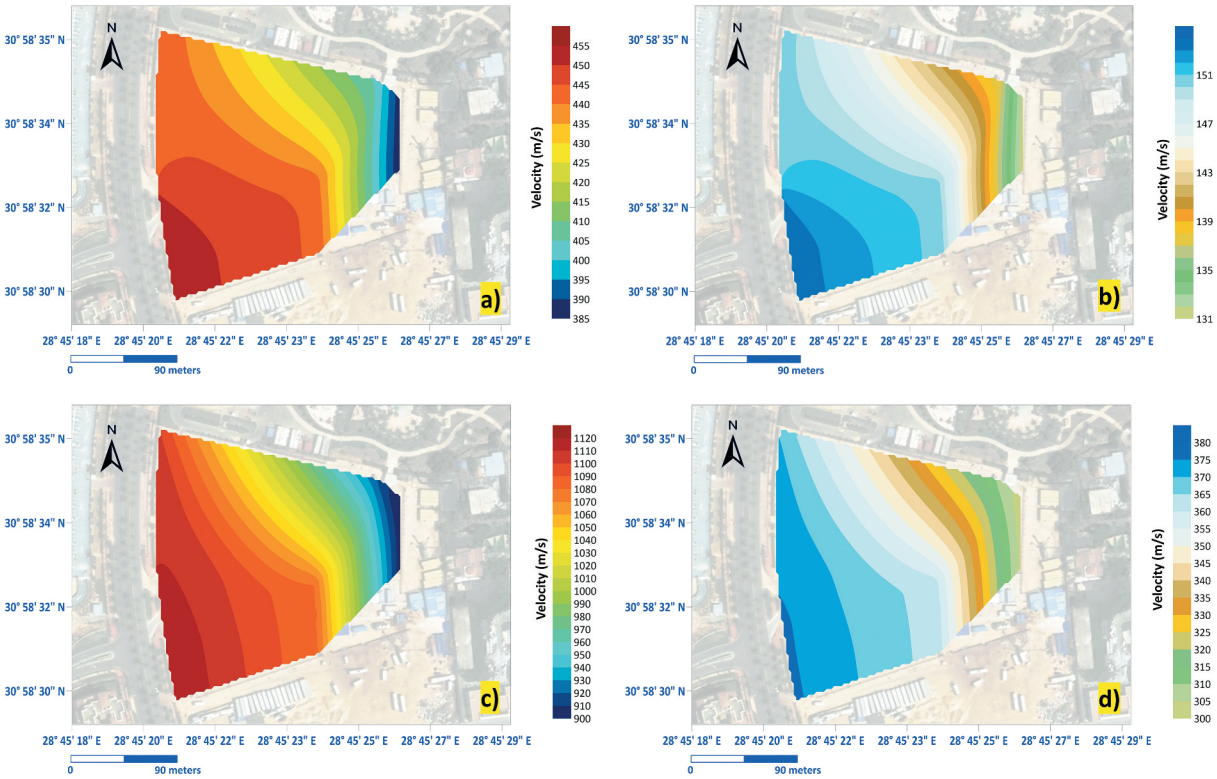

Figure 6. The distribution map of (a) Vp in the first layer, (b) Vs in the first layer, (c) Vp in the second layer, and (d) Vs in the second layer.

the second layer, it is ranging between 980 in the eastern part and 1560 Dyn/Cm^2 in the southwestern part of the study area (Figure 7(b)).

The Standard of the Penetration Test (SPT) or (N value) is geotechnically known as the resistivity for penetration by normalised cylindrical bars under standard load. The following equation of Stumpel et al. (1984) has been used to calculate this value:

$$Vs = 89.9N^{0.341} \quad (2)$$

According to the classification of Bowles (1984), the N values in the first layer, which are varying from 3 to 5, refer to loose and soft soil, the low values locate in the eastern part, and it increases gently to the southwestern part of the study area (Figure 7(c)). The values of N of the second layer record values of about 34 in

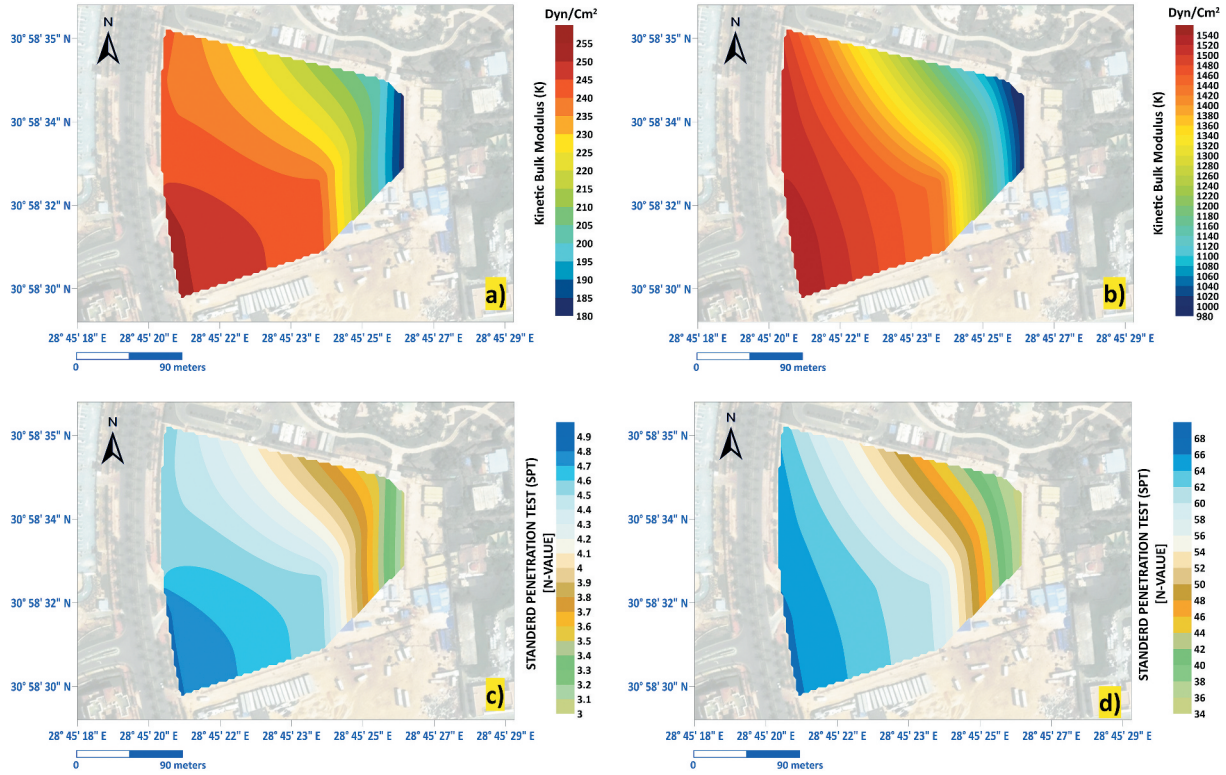

Figure 7. The distribution map of (a) Kinetic Bulk modulus (K) in the first layer, (b) Kinetic Bulk modulus (K) in the second layer, (c) Standard of the Penetration Test (SPT) or (N value) in the first layer, and (d) Standard of the Penetration Test (SPT) or (N value) in the second layer.

the eastern part, this indicates dense and solid soil. The values increase until reach about 69 in the southwestern part of the study area; this indicates very dense and solid soils on this side (Figure 7(d)).

4.2.3. Material competence scales

Soil compaction stratum is considered to a great extent as a measure of the degree of competence for foundation and other civil engineering purposes. It depends on both the elastic moduli of the soil and the pressure distribution at their depth. The following equation of Martin 1984 has been used to calculate this value:

$$\mathrm{Ci} = \left[3 - 4\left(\mathrm{Vs}^2/\mathrm{Vp}^2\right)\right] / \left[1 - 2\left(\mathrm{Vs}^2/\mathrm{Vp}^2\right)\right] \quad (3)$$

The value of concentration index (Ci) in the first layer ranges between 3.298 and 3.301 (Figure 8(a)). In the second layer, this index is ranging between from 3.29 to 3.292 (Figure 8(b)). The low values in the southwestern part indicate a relatively low competent to moderately competent material. While the high values tend to appear in the eastern portion of the study area, they indicate moderately competent to competent materials. The convergence of the (Ci) values may be due to the majority of the material constituting the sand layers (Shipton and Coop 2015), and the simple differences are due to the overlap of some other rocky components, such as clay and silt, but in simple proportions, or a change in the size of sand grains, or an increase in the vertical load on the lower layers (Basu et al. 2008; Gupta and Basu 2017).

The stress ratio (Si) can be obtained by dividing the horizontal stress and vertical stress, and it refers to competence of material scale. The following equation of Tatham and Krug (1986) has been used to calculate this value:

$$\mathrm{Si} = 1 - 2\left(\mathrm{Vs}^2/\mathrm{Vp}^2\right) \quad (4)$$

This value is varying from 0.768 to 0.77 in the first layer (Figure 8(c)), while this value is varying from 0.773 to 0.774 in the second layer (Figure 8(d)). According to the classification scale of Kanazawa and Machida (1975), the low values occupying the eastern part indicate that they are relatively less compact than semi-moderate materials. The high values are observed in the southwestern part of the study area, and they reflect moderate to compact material. The combination of the values is due to the similar sand nature of the two layers forming material (Massarsch et al. 2021). The reason for the slight difference is due to the change in the vertical weight, especially on the parts accumulated above the lower layer (Stapelfeldt et al. 2021).

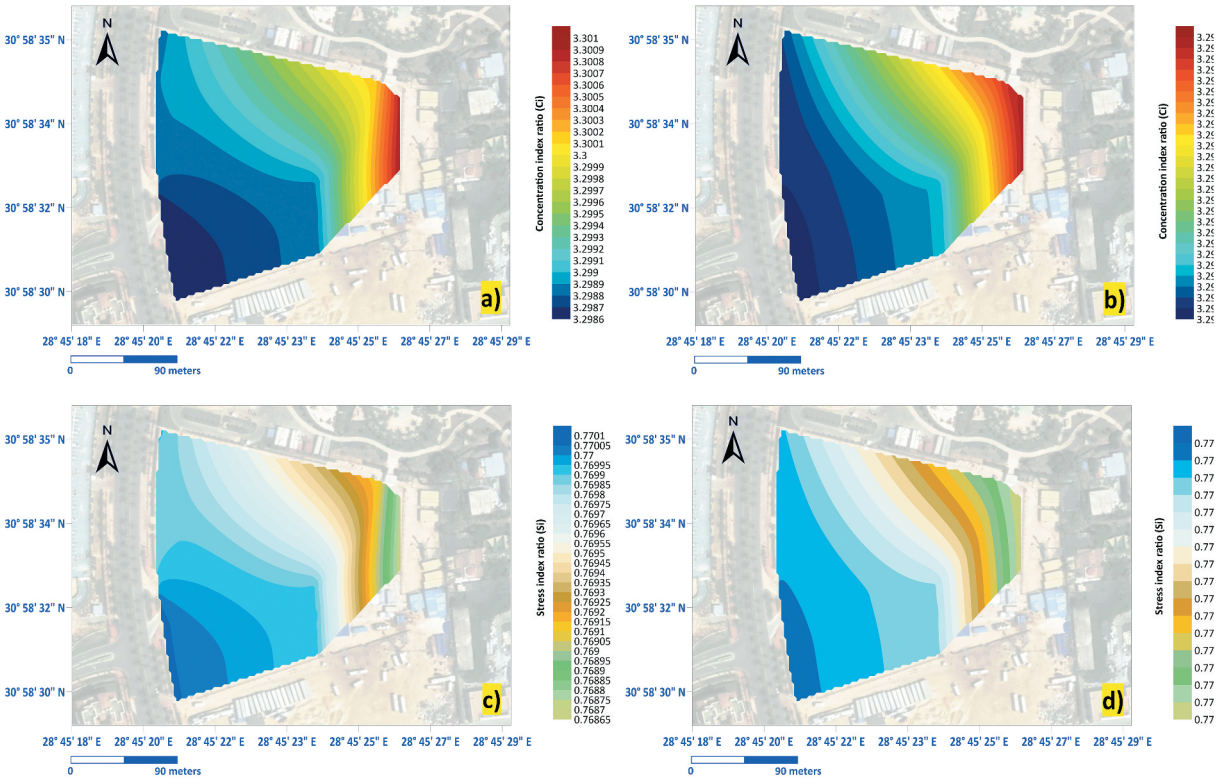

Figure 8. The distribution map of (a) concentration index (Ci) in the first layer, (b) concentration index (Ci) in the second layer, (c) stress ratio (Si) in the first layer, and (d) stress ratio (Si) in the second layer.

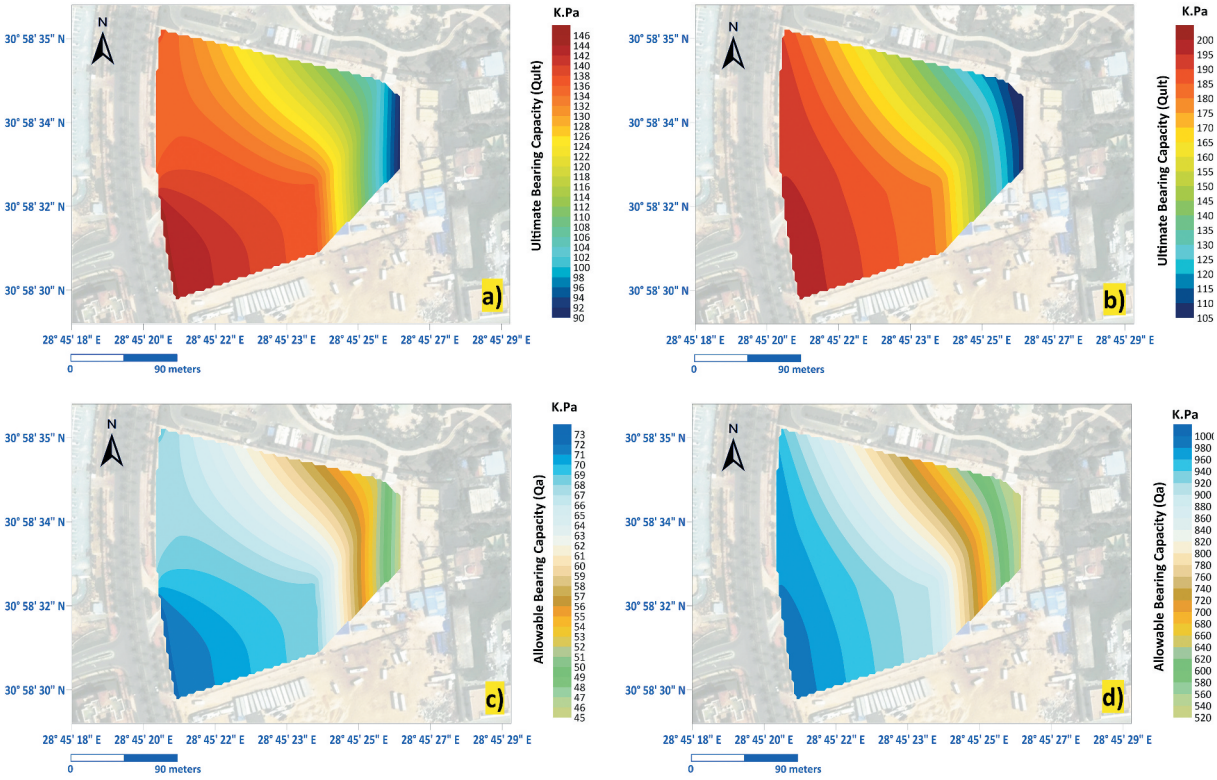

Figure 9. The distribution map of (a) ultimate bearing capacity (Qult) in the first layer, (b) ultimate bearing capacity (Qult) in the second layer, (c) allowable bearing capacity (Qa) in the first layer, and (d) allowable bearing capacity (Qa) in the second layer.

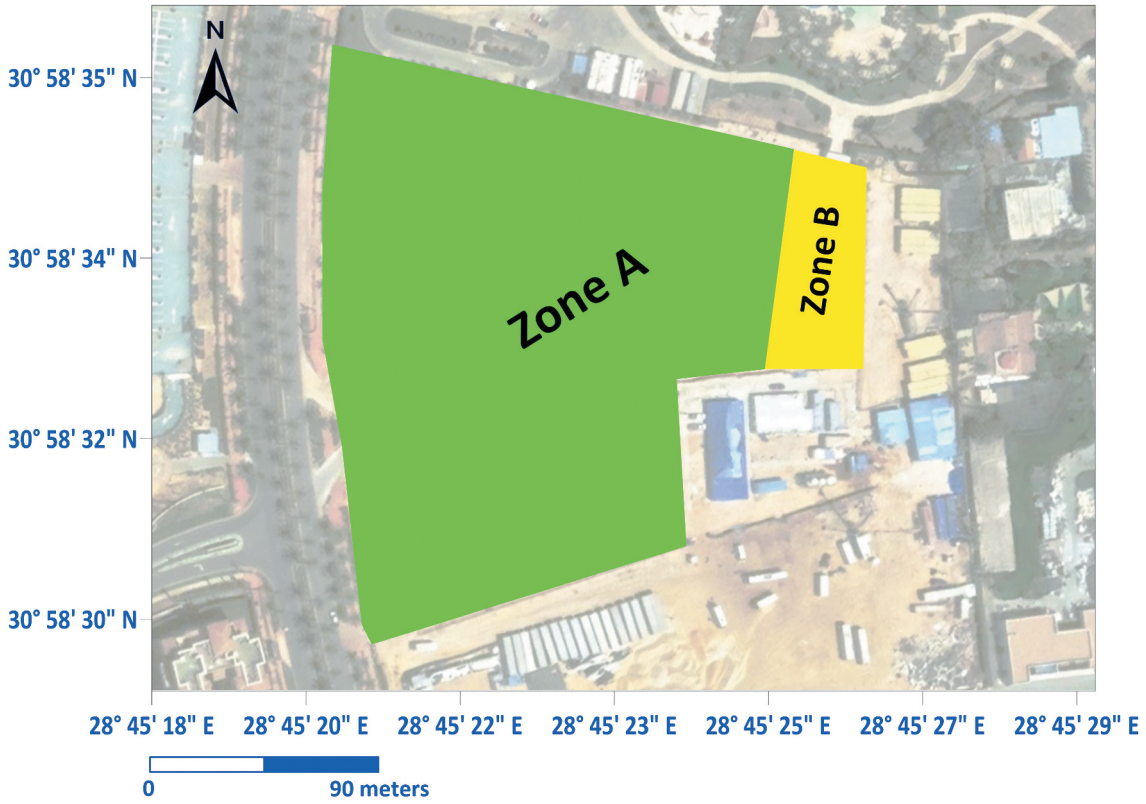

Figure 10. Zonation map of the study area.

4.2.4. Foundation material bearing capacity

The ultimate bearing capacity (Qult) expresses the maximum load required for shear failure or sand liquefaction. This capacity is controlled by shear strength factor. The following equation of Bowles (1988) has been used to calculate this value:

$$Q_{ult} = 10^{2.932(\log Vs - 1.45)} \quad (5)$$

The ultimate bearing capacity of the surface first layer is varying between 90 K.Pa in the eastern part and 148 K.Pa in the southwestern part (Figure 9(a)). The value of the ultimate bearing capacity in the second layer varies between 1050 K.Pa in the eastern part and 2050 K.Pa in the southwestern part (Figure 9(b)).

The allowable bearing capacity (Qa) is the maximum load to be considerable to avoid shear failure or sand liquefaction (Fuliang 1982). It can also be termed as allowable bearing pressure; the foundation materials are affected by both strength and deformation characteristics. The following equation of Georgiadis and Butterfield (1988) has been used to calculate this value:

$$Qa = Q_{ult}/F \quad (6)$$

The safety factor (F) equals 2 when the soil is cohesionless and equals 3 when the soil is a cohesive material. The parameter values are ranging from 45 K.Pa in the eastern part to 74 K.Pa in the southwestern part of the first layer (Figure 9(c)), while they range from 520 K.Pa in the eastern part to 1020 K.Pa in the southwestern part of the second layer (Figure 9(d)).

5. Discussion and recommendations

It is clear from the previously interpreted data of ERT that there are two distinct layers for the study area. The ERT method is characterised by the fact that it clearly shows the sea- watersea-water interference in the second layer on the eastern side of the study area. This interference begins to appear on the eastern side only (approximately 50 metres in horizontal length, starting from the east side) at a depth of about 27 m to the end of the measured profile. There is a slight appearance of some lithological changes in the second layer that may be due to the presence of muddy or clayey lenses, but with simple sizes and diameters.

The data interpretations of the SSR method showed that there are also two layers that characterise the study area. Although the thickness of the layers in this method differs from the ERT method, despite the difference in thickness values, this difference does not seem large, but it can be distinguished. This difference is due to the different physical properties on which each measurement method depends.

Depending on the geotechnical calculations, the study area can be divided into two zones (Figure 10). The first (A) zone extends over the entire western part, the middle, and part of the eastern side. This zone covers most of the study area. In this zone, the first surface layer is composed of materials with medium hardness, cohesion, and stability, while the second layer consists of materials with good hardness,

cohesion, and stability. It is recommended to erect structures and buildings with small and medium heights, after removing the surface layer and starting to the architectural foundations in the second layer.

The second (B) zone is in the far eastern part of the study area and covers a percentage not exceeding 14% of the study area. The first layer in this zone is an extension of the first layer in the first (A) zone, but with an increase in the thickness, while, the second layer, despite being of the same components as the second layer found in the first (A) zone, loses many of its properties. This can be attributed to the effect of the intrusion of sea water from this side, which increases the disintegration of soil particles and increases the porosity and permeability. This intrusion will affect the stability of the soil and may lead to the flow of sea water to the surface by the effects of tidal movements in hurricane seasons, and it will also have a major role in the process of eroding the iron used in the architectural foundations. It is recommended to exclude this area from any buildings and construction. This zone can be used to make swimming pools, decorative agricultural areas, or water fountains.

Disclosure statement

No potential conflict of interest was reported by the author(s).

ORCID

Alhussein Adham Basheer http://orcid.org/0000-0001-5283-9201

References

[EGPC] Egyptian General Petroleum Corporation. 1984. Well evaluation conference of Egypt. Schlumberger Technical Editing Services. Egypt: EGPC; p. 64.

Adepelumi AA, Ako BD, Ajayi TR, Afolabi O, Omotoso EJ. 2009. Delineation of saltwater intrusion into the freshwater aquifer of Lekki Peninsula, Lagos, Nigeria. Environ Geol. 56(5):927–933. doi:10.1007/s00254-008-1194-3.

Alabjah B, Amraoui F, Chibout M, Slimani M. 2018. Assessment of saltwater contamination extent in the coastal aquifers of Chaouia (Morocco) using the electric recognition. J Hydrol. 566:363–376. doi:10.1016/j.jhydrol.2018.09.003.

Alshehri F, Almadani S, El-Sorogy AS, Alwaqdani E, Alfaifi HJ, Alharbi T. 2021. Influence of seawater intrusion and heavy metals contamination on groundwater quality, Red Sea coast, Saudi Arabia. Mar Pollut Bull. 165:112094. doi:10.1016/j.marpolbul.2021.112094.

Bader Petroleum Company "BAPETCO". 2007. Generalized Litho-Stratigraphic Column of Western Desert. Internal report. p. 10.

Basheer AA, Abdelmotaal AM, Mesbah HS, Mansour KK. 2014a. Application of geophysical methods for geotechnical parameters determination at New Borg El-Arab industrial City, Egypt. Curr Urban Stud English. 2(1): P.17. ISSN: 2328-4900. doi:10.4236/cus.2014.21003. March 2014.

Basheer AA, Atya MA, Shokri M, Abu Shady MM. 2012. Application of ERT and SSR to detect the subsurface cave at 15th May City, Helwan, Egypt. NRIAG J Astron Geophys. 1(1):23–32. doi:10.1016/j.nrjag.2012.11.003.

Basheer AA, Taha AI, Mansour KQ, Khalil A, Rabeh T. 2014b. Assessment of the saline-water intrusion through the fresh groundwater aquifer by using ER and TEM methods at the Qantara Shark Area, Sinai Peninsula, Egypt. Int J Innovative Res Dev. 3(4):398–406.

Basu D, Salgado R, Prezzi M. 2008. Analysis of laterally loaded piles in multilayered soil deposits. Joint Transport Res Program. 23:330.

Bowles JE. 1984. Physical and Geotechnical properties of soil. 330 West 42nd Street, New York, NY United States 10036: McGraw-Hill London; p. 477–480.

Bowles JE. 1988. Foundation analysis and design. Shoppenhangers Road, Maidenhead, Berkshire SL6 2QL, England: McGraw-Hill Book Company Limited, England.

Butzer KW. 1960. On the Pleistocene shore lines of Arabs' gulf, Egypt. J Geol. 68(6):626–637. doi:10.1086/626701.

Červený V, Molotkov IA, Pšenčík I, Vaněk J. 1982. Space-time ray method for seismic wave fields. Studia Geophysica Et Geodaetica. 26(4):342–351. doi:10.1007/BF01639635.

Comina C, Mandrone G, Arato A, Chicco J, Duò E, Vacha D. 2021. Preliminary analyses of an innovative soil improving system by sand/gravel injections–Geotechnical and geophysical characterization of a first test site. Eng Geol. 106278. doi:10.1016/j.enggeo.2021.106278.

Dutta NP. 1984. Seismic refraction method to study the foundation rock of a dam. Geophys Prospect. 32 (6):1103–1110. doi:10.1111/j.1365-2478.1984.tb00757.x.

Edwards JT, Hillel AJ. 1977. The electrical resistivity of GP zones. Philos Mag. 35(5):1221–1229. doi:10.1080/14786437708232948.

El Bastawesy MA, Nasr A, Ali RR. 2008. The use of remote sensing and GIS for catchment delineation in northwestern coast of Egypt: an assessment of water resources and soil potential. Egypt J Remote Sens Space Sci. 11:3–16.

Fat-Helbary RES, El-Faragawy KO, Hamed A. 2019. Soil geotechnical characteristics for seismic risk mitigation at the southern extension of Marsa Alam city, Egypt. NRIAG J Astron Geophys. 8(1):1–14. doi:10.1080/20909977.2019.1588676.

Fehlberg H, Stahr K. 1985. Development of sustained land use by understanding soil and landscape formation in the desert fringe area of NW-Egypt. Catena. 12(4):307–328. doi:10.1016/0341-8162(85)90021-9.

Fuliang LSZXZ. 1982. Determination of static bearing capacity of single pile by wave equation using input of direct force wave measurement. J Build Struct. 2:3–16. 1110-9823.

Georgiadis M, Butterfield R. 1988. Displacements of footings on sand under eccentric and inclined loads. Can Geotech J. 25(2):199–212. doi:10.1139/t88-024.

Goebel M, Pidlisecky A, Knight R. 2017. Resistivity imaging reveals complex pattern of saltwater intrusion along Monterey coast. J Hydrol. 551:746–755. doi:10.1016/j.jhydrol.2017.02.037.

Gordon J, Gillespie D, Potter J, Frantzis A, Simmonds MP, Swift R, Thompson D. 2003. A review of the effects of seismic surveys on marine mammals. Mar Technol Soc J. 37(4):16–34. doi:10.4031/002533203787536998.

Griffiths DH, Barker RD. 1993. Two-dimensional resistivity imaging and modelling in areas of complex geology. J Appl Geophys. 29(3–4):211–226. doi:10.1016/0926-9851(93)90005-J.

Gupta BK, Basu D. 2017. Analysis of laterally loaded short and long piles in multilayered heterogeneous elastic soil. Soils Found. 57(1):92–110. doi:10.1016/j.sandf.2017.01.007.
Hawkins LV. 1961. The reciprocal method of routine shallow seismic refraction investigations. Geophysics. 26 (6):806–819. doi:10.1190/1.1438961.
Kanazawa T, Machida S. 1975. On the effect of cyclic stress ratio on the fatigue crack propagation. Eng Fract Mech. 7 (3):445–455. doi:10.1016/0013-7944(75)90045-4.
Kazakis N, Pavlou A, Vargemezis G, Voudouris KS, Soulios G, Pliakas F, Tsokas G. 2016. Seawater intrusion mapping using electrical resistivity tomography and hydrochemical data. An application in the coastal area of eastern Thermaikos Gulf, Greece. Sci Total Environ. 543:373–387. doi:10.1016/j.scitotenv.2015.11.041.
Kouzana L, Benassi R. 2010. Geophysical and hydrochemical study of the seawater intrusion in Mediterranean semi arid zones. Case of the Korba coastal aquifer (Cap-Bon, Tunisia). J Afr Earth Sci. 58(2):242–254. doi:10.1016/j.jafrearsci.2010.03.005.
Le Pichon X, Şengör AC, İmren C. 2019. A new approach to the opening of the eastern Mediterranean Sea and the origin of the Hellenic Subduction Zone. Part 1: the eastern Mediterranean Sea. Can J Earth Sci. 56 (11):1119–1143. doi:10.1139/cjes-2018-0128.
Loke MH, Acworth I, Dahlin T. 2003. A comparison of smooth and blocky inversion methods in 2D electrical imaging surveys. Explor Geophys. 34(3):182–187. doi:10.1071/EG03182.
Martínez-Moreno A. 2017. Calidad en el deporte de élite. Análisis de fortalezas y debilidades psicológicas en jugadores de balonmano. Cuadernos de Psicología Del Deporte. 17(1):19–24.
Massarsch KR, Wersäll C, Fellenius BH. 2021. Liquefaction induced by deep vertical vibratory compaction. Proc Inst Civil Engineers-Ground Improv. 174(3):194–205. doi:10.1680/jgrim.19.00018.
McInnis D, Silliman S, Boukari M, Yalo N, Orou-Pete S, Fertenbaugh C, Fayomi H. 2013. Combined application of electrical resistivity and shallow groundwater sampling to assess salinity in a shallow coastal aquifer in Benin, West Africa. J Hydrol. 505:335–345. doi:10.1016/j.jhydrol.2013.10.014.
Meshref WM. 1995. Well evaluation conference of Egypt. Schlumberger Technical Editing Services. Egypt: EGPC; p. 87.
Nowroozi AA, Horrocks SB, Henderson P. 1999. Saltwater intrusion into the freshwater aquifer in the eastern shore of Virginia: a reconnaissance electrical resistivity survey. J Appl Geophys. 42(1):1–22. doi:10.1016/S0926-9851(99)00004-X.
Palmer D. 1980. The generalized reciprocal method of seismic refraction interpretation. Tulsa, Oklahoma: Society of Exploration Geophysicists. doi:10.1190/1.9781560802426.
Prodehl C, Fuchs K, Mechie J. 1997. Seismic-refraction studies of the Afro-Arabian rift system—a brief review. Tectonophysics. 278(1–4):1–13. doi:10.1016/S0040-1951(97)00091-7.
Ray R, Kumar D, Samui P, Roy LB, Goh ATC, Zhang W. 2021. Application of soft computing techniques for shallow foundation reliability in geotechnical engineering. Geosci Front. 12(1):375–383. doi:10.1016/j.gsf.2020.05.003.
Res2Dinv software. 3.59, Geotomo Inc. https://www.geotomosoft.com/downloads.php .
Royden LH, Papanikolaou DJ. 2011. Slab segmentation and late Cenozoic disruption of the Hellenic arc. Geochem Geophys Geosyst. 12(3). doi:10.1029/2010GC003280.
Said R. 1962. The geology of Egypt. Amesterdam: Elsevier Pub. Comp.
Said R. 1990. The geology of Egypt. New York (NY): Elsevier Publ. Co.; p. 377.
Sakr MA, Omar AE, Saad AM, Moayedi H. 2021. Geotechnical parameters modelling and the radiation safety of expansive clayey soil treated with waste marble powder: a case study at west Gulf of Suez, Egypt. Environ Earth Sci. 80(7):1–18. doi:10.1007/s12665-021-09573-y.
Salama T, Karam M, Hegazi A. 2020. Geotechnical evaluation of soil at el-alamein new city, Northern Coast, Egypt. J Pet Min Eng. 22(1):26–34. doi:10.21608/jpme.2020.23635.1026.
Satheeskumar V, Subramani T, Lakshumanan C, Roy PD, Karunanidhi D. 2021. Groundwater chemistry and demarcation of seawater intrusion zones in the Thamirabarani delta of south India based on geochemical signatures. Environ Geochem Health. 43(2):757–770. doi:10.1007/s10653-020-00536-z.
Seisimager/2D. https://www.geometrics.com/software/seisimager-2d .
Seisviewer. Seismic software by Schlumberger . https://www.software.slb.com/products .
Sheriff RE. 1991. Encyclopedic dictionary of exploration geophysics. 3rd ed. Tulsa, Oklahoma: Society of Exploration Geophysicists.
Shipton B, Coop MR. 2015. Transitional behaviour in sands with plastic and non-plastic fines. Soils Found. 55 (1):1–16. doi:10.1016/j.sandf.2014.12.001.
Shukri NM, Philip G, Said R. 1955. *The geology of Mediterranean coast between Rosetta and Bardia, Part 2, Pleistocene sediments, Geomorphology and microfacies*. Bull Inst D' Egypt. 37(2):*395–42*.
Shynkarenko A, Lontsi AM, Kremer K, Bergamo P, Hobiger M, Hallo M, Fäh D. 2021. Investigating the subsurface in a shallow water environment using array and single-station ambient vibration techniques. Geophys J Int. 227(3):1857–1878. doi:10.1093/gji/ggab314.
SIP Seismic image Processing. https://www.seismicimageprocessing.com/ .
Sjogren B, Ed. 2013. Shallow refraction seismics. Berlin, Heidelberg, Germany: Springer Science & Business Media.
Stapelfeldt M, Bienen B, Grabe J. 2021. Influence of low-permeability layers on the installation and the response to vertical cyclic loading of suction caissons. J Geotech Geoenviron Eng. 147(8):04021076. doi:10.1061/(ASCE)GT.1943-5606.0002522.
StrataVisor NZXP. https://www.geometrics.com/product/stratavisor-nzxp/ .
Stumpel H, Kahler S, Meer R, Milkerei B. 1984. The use of seismic shear waves and compressional waves for lithological problems of shallow sediments. Geoph Pros. 32:660–675.
Sultan N, Halim A. 1988. Tectonic framework of northern Western Desert, Egypt and its effect on hydrocarbon accumulations. In: EGPC 9th Exploration Conference. Cairo, Egypt.
Syscal Pro. http://www.iris-instruments.com/syscal-pro.html .
Tatham RH, Krug EH. 1986. Vp/Vs Interpretation. Ch. 5. In: Fitch AA, editor. Developments in Geophysical Exploration Methods-6. London: Elsevier Applied Science Publishers; p. 139–188, 264.
White RMS, Collins S, Loke MH. 2003. Resistivity and IP arrays, optimised for data collection and inversion. ASEG Extended Abstr. 2003(2):1–4. doi:10.1071/ASEG2003ab182.
Zahran AA. 2008. Geotechnical study of Carbonate rocks on the area between Alexandria and El Alamein along The Mediterranean Sea Coast of Egypt. Ass Univ Bull Environ Res. 11(1):12.